Neurosurg Rev (2015) 38:739–751
DOI 10.1007/s10143-015-0643-1

ORIGINAL ARTICLE

Assessment of a method to determine deep brain stimulation targets using deterministic tractography in a navigation system

Josué M. Avecillas-Chasin[1] · Fernando Alonso-Frech[2] · Olga Parras[3] · Nayade del Prado[4] · Juan A. Barcia[1,3]

Received: 14 July 2014 / Revised: 4 February 2015 / Accepted: 14 March 2015 / Published online: 12 May 2015

Abstract Recent advances in imaging permit radiologic identification of target structures for deep brain stimulation (DBS) for movement disorders. However, these methods cannot detect the internal subdivision and thus cannot determine the appropriate DBS target located within those subdivisions. The aim of this study is to provide a straightforward method to obtain an optimized target (OT) within DBS target nuclei using a widely available navigation system. We used T1- and T2-weighted images, fluid-attenuated inversion recovery (FLAIR) sequence, and diffusion tensor imaging (DTI) of nine patients operated for DBS in our center. Using the StealthViz® software, we segmented the targeted deep structures (*subcortical targets*) and the anatomically identifiable areas to which these target nuclei were connected (*projection areas*). We generated fiber tracts from the projection areas. By identifying their intersections with the subcortical targets, we obtained an OT within the DBS target nuclei. We computed the distances from the clinically effective electrode contacts (CEEC) to the OT obtained by our method and the targets provided by the atlas. These distances were compared using a Wilcoxon signed-rank test, with $p<0.05$ considered statistically significant. We were able to identify OT coincident with the motor part of the subthalamic nucleus and the ventral intermediate nucleus. We clinically tested the results and found that the CEEC were significantly more closely related to the OT than with the targets obtained by the atlas. Our present results show that this novel method permits optimization of the stimulation site within the internal subdivisions of target nuclei for DBS.

Keywords Deep brain stimulation · Structural connectivity · Parcellation · Basal ganglia · Cortical segmentation · Individualized targeting

✉ Juan A. Barcia
jabarcia@med.ucm.es

[1] Department of Neurosurgery, Institute of Neurosciences, Instituto de Investigación Sanitaria San Carlos, Hospital Clínico San Carlos, Prof. Martín Lagos s/n, 28040 Madrid, Spain

[2] Department of Neurology, Hospital Clínico San Carlos, Madrid, Spain

[3] Department of Surgery, Universidad Complutense de Madrid, Madrid, Spain

[4] Unidad de Metodología de Investigación y Epidemiología Clínica, Unidad de Gestión Clínica de Medicina Preventiva, Hospital Clínico San Carlos, Instituto de Investigación Sanitaria del Hospital Clínico San Carlos (IdISSC), Madrid, Spain

Introduction

Deep brain stimulation (DBS) is an effective method for treating the most disabling symptoms of certain movement disorders [15, 17, 23, 39, 40]. Such treatments have involved modulation of several different nuclei, including the subthalamic nucleus (STN) and nucleus ventralis intermedius (VIM) of the thalamus [2, 7, 39, 40, 59].

Targets have traditionally been selected through the anterior commissure-posterior commissure (AC-PC) reference system, which is further refined by neurophysiologic microelectrode recording (MER) and macroelectrode stimulation to ensure electrode localization at the optimal site for clinical improvement. In up to 50 % of cases, the radiologically defined first trajectory for the STN is deemed unreliable based on neurophysiologic results and has to be modified, lengthening the procedure's duration and thus increasing patient's fatigue (awake surgery), and possibly the risk of morbidity [66]. Also, some authors have found a discrepancy greater than 1.5 mm (corresponding to the radius of the sphere of the effective

electric field generated by the stimulator) between the radiologically defined target and the one obtained by the microrecordings [31]. Some brain structures can be easily identified using current brain imaging methods, and it is possible to choose targets directly based on such images [2, 62, 71]. However, the optimal electrode position for DBS is at a functional "sub-structure" within target nuclei (herein referred to as an optimized target (OT)); for example, the precise stimulation site for motor symptoms of Parkinson's disease (PD) is the motor subdivision of the STN located at its dorsolateral region [34, 40, 50, 53, 64].

Tractography is a technique based on diffusion tensor imaging (DTI), which has been used to non-invasively reconstruct white matter pathways in the brain [8, 45, 68]. DTI deterministic tractography (DTI-DT) estimates the neural connections by designating at least two regions of interest (ROI) in the 3-dimensional (3D) space [68]. The DTI software StealthViz® (Medtronic, MN, USA) is based on the fiber assignment by continuous tracking (FACT) algorithm [37, 45] for white matter tract reconstruction and is widely used for surgical planning in clinical practice. Here, we present a method using DTI-DT, MRI sequences available in clinical practice, and StealthStation® navigation software that allows the localization of different DBS target subdivisions through basal ganglia circuit segmentation to provide an OT, although this method is not intended to replace the intraoperative MER and macrostimulation to further refine the final stimulation site. In this paper, we describe this method and compare the accuracy of the OT obtained by tractography with the atlas-based targets.

Material and methods

Patients

We used the imaging studies of nine patients who were operated for DBS in our center from 2011 to 2014. We selected those patients who had undergone diffusion MR imaging according to the protocol specified subsequently, prior to the DBS system implantation. Clinical and demographic data including the preoperative clinical status, stimulation parameters, postoperative clinical outcome, and follow-up were recorded (Table 1). All patients provided consent for analysis and publication of their data.

Data acquisition

All MRI studies were performed using a 3 T clinical imager (Signa HDXt GE Healthcare) with an eight-channel head coil. The imaging protocol was the same for all patients. The T2-weighted fast spin-echo sequence was acquired with the following parameters: repetition time (TR), 6000 ms; echo time (TE), 95 ms; field of view (FOV), 220 mm; interpolated matrix, 512×512; and slice thickness, 1 mm. The T1-weighted 3-dimensional Fast SPGR IRprep sequence was acquired with the following parameters: TR, 8 ms; TE, 2 ms; flip angle, 12; FOV, 240 mm; matrix, 256×256; slices, 160; slice thickness, 1 mm; inversion time (TI), 450 ms; and isotropic voxels, 1 mm. The FLAIR-FSE 3D sequence was acquired with the following parameters: TR, 6600 ms; TE, 110 ms; TI, 2200 ms; FOV, 240 mm; matrix, 256×256; slices, 160; and slice thickness, 1 mm. These parameters enabled reconstruction with a 1-mm isotropic voxel size. Diffusion weighting was encoded along 55 independent orientations using a single-shot multi-slice 2D spin-echo diffusion-sensitized and fat-suppressed echo planar imaging (EPI) sequence, with b values of 0–1000 mm^2/s, TR/TE of 9600/82 ms, FOV of 250×250 mm, matrix of 96×96, and slice thickness of 2.6 mm with no inter-slice gap, resulting in isotropic voxels of 2.6 mm. FUNCTOOL software (General Electric HC) was used to improve geometric distortion. Preoperative and postoperative computed tomography (CT) scans were acquired on a multi-slice Philips ® Brilliance 64 with spiral pitch of 0.891, rotation of 0.75 s, no gantry tilt, matrix of 512×512, slice thickness of 1 mm, tube voltage of 120 kV, and tube current of 75 mA.

Regions of interest

Several cortical and subcortical structures involved in extrapyramidal circuits were defined as ROIs for DTI generation and were classified as *projection areas* and *subcortical targets*. The following were included as projection areas: primary motor cortex (M1, Brodmann area 4); supplementary motor area (SMA, part of Brodmann area 6) [30, 46]; pre-supplementary motor area (pre-SMA, Brodmann area 6 and part of 8) [30, 46, 69]; red nucleus (RN); and dentate nucleus (DN). The subcortical targets included the thalamus (Th) and the subthalamic nucleus (STN) (Fig. 1).

Delineation of projection areas and subcortical targets (manual segmentation)

This process was performed with a StealthStation® (Medtronic, MN, USA) and the StealthViz® software package (Medtronic), using the "segmentation section" of the software. Projection areas segmentation was performed by manually tracing the cortical segment boundaries based on Brodmann areas. Subcortical target segmentation was performed manually on the MR sequence in which the structure was most clearly defined (Fig. 1). We used several neuroanatomical sources to guide the delineation of neuroanatomical ROIs on MRI images [24, 25, 30, 38, 42, 46, 48, 63, 70].

Table 1 Clinical and demographic data of the patients, stimulation features, clinical outcome, and follow-up

Patients	Age/gender/ diagnosis	Clinical features, pre-DBS	Target	Traj. No.	CEEC	Parameters (v-ms-Hz)	Clinical outcome, post-DBS	Follow-up (mo)
1	47/F/PD	UPDRS off-med: 37	STN	2L, 2R	L 0 **1** 2 3 R 8 9 10 **11**	L: 2.5-90-130 R: 2.2-90-130	UPDRS off-med: 8	15
2	54/M/PD	UPDRS off-med: 39	STN	6L, 4R	L 0 1 2 **3** R 8 **9** 10 11	L: 2.7-60-160 R: 2.7-60-160	UPDRS off-med: 23	10
3	64/M/PD	UPDRS off-med: 28	STN	2L, 3R	L 0 1 **2** 3 R 8 9 **10** 11	L: 3.5-90-130 R: 4.0-90-130	UPDRS off-med: 8	6
4	60/M/PD	UPDRS off-med: 18	STN	2L, 1R	L 0 1 **2 3** R 8 9 **10 11**	L: 1.2-90-130 R: 1.5-90-130	UPDRS off-med: 6	5
5	70/M/PD	UPDRS off-med: 42	STN	2L, 2R	L 0 1 2 **3** R 8 **9** 10 11	L: 3.0-60-130 R: 2.5-60-130	UPDRS off-med: 25	4
6	58/F/PD	UPDRS off-med: 50	STN	2L, 3R	L 0 1 2 **3** R 8 9 10 **11**	L: 3.0-60-130 R: 3.0-60-130	UPDRS off-med: 13	3
7	68/M/ET	FTM: 61	VIM B	3L, 2R	L 0 **1** 2 3 R 8 **9** 10 11	L: 2.8-60-190 R: 3.0-60-190	FTM: 10	16
8	69/F/ET	FTM: 49	VIM B	3L, 3R	L 0 1 **2 3** R 8 9 **10 11**	L: 3.0-60-130 R: 3.5-60-130	FTM: 8	7
9	40/M/ET	FTM: 47	VIM B	4L, 4R	L 0 1 **2** 3 R 8 9 10 **11**	L: 4.0-60-180 R: 2.7-60-180	FTM: 24	3

Clinically effective electrode contacts (CEEC) are shown in bold

DBS deep brain stimulation, *F* female, *M* male, *PD* Parkinson's disease, *ET* essential tremor, *UPDRS* unified Parkinson's disease rating scale, *FTM* Fahn-Tolosa-Marin scale, *STN* subthalamic nucleus, *VIM B* bilateral ventral intermediate nucleus, *Traj* Trajectories, *L* left, *R* right, *CEEC* clinically effective electrode contacts, *v-ms-Hz* volts-milliseconds-hertz, *mo* months

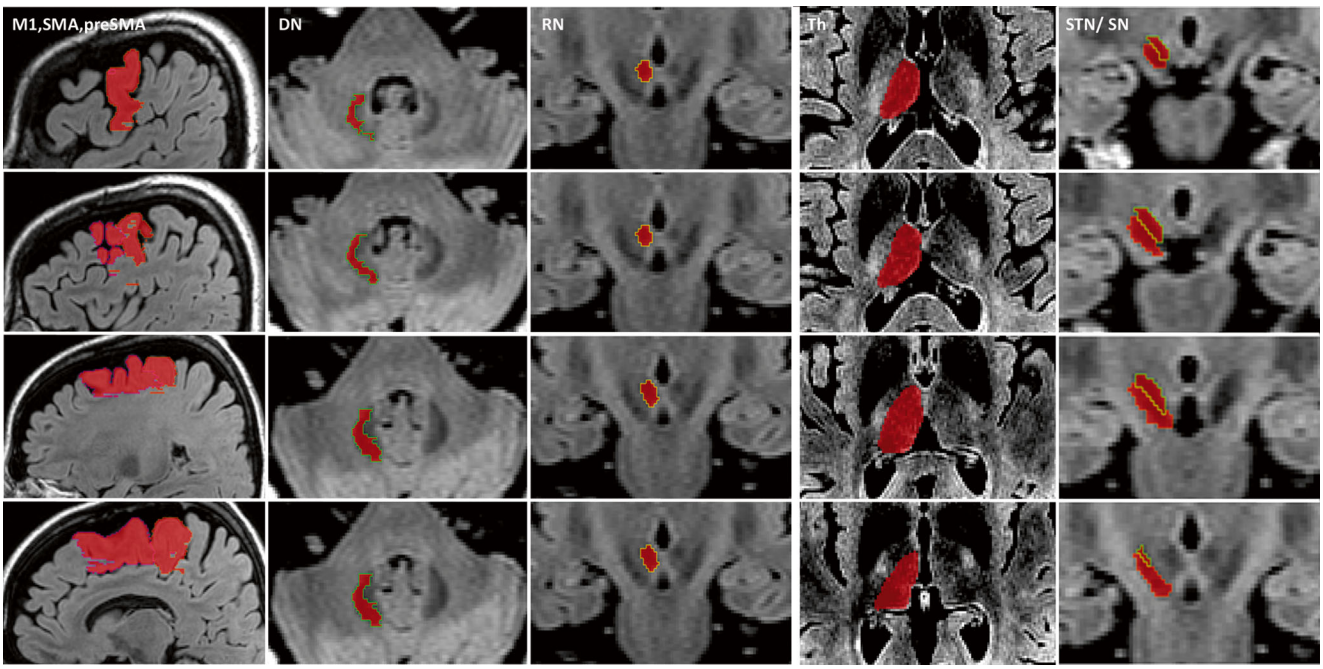

Fig. 1 Anatomical boundaries of the regions of interest: projection areas (*M1* motor cortex, *SMA* supplementary motor area, *pre-SMA* pre-supplementary motor area, *DN* dentate nucleus, *RN* red nucleus) and subcortical targets (*Th* thalamus, *STN* subthalamic nucleus) segmented manually in FLAIR 3D and T1 sequences. These are sequences commonly used in clinical practice that we found adequate to define the boundaries of the subcortical ROIs. Other sequences are used for this aim, but our approach takes advantage of readily available studies performed in the clinical setting. The *Th* is difficult to define in MRI due to the poor between-tissue contrast at the thalamic gray-white matter interface. By adjusting the contrast in T1-weighted images, we were able to obtain the lateral limit of the thalamus defined by the posterior limb of the internal capsule. Finally, we used the 3D FLAIR sequence to obtain the maximal resolution of the voxels for structures such as STN and SN. The substantia nigra (*SN*) was also segmented to obtain the antero-inferior boundary of the STN

Deterministic tractography processing and analysis

Tractography was processed using the FACT algorithm [37] with a StealthStation® and the StealthViz® software package. The fractional anisotropy (FA) "start value" and "stop value" were not less than 0.1, and the maximal directional change of fibers was set as 45 to 80°. These values were chosen after a thorough analysis of the fiber tracking and plausibility of the results according to previous reports [4, 6, 7, 9, 11, 19, 20, 26, 32, 38, 41, 42, 70].

Parcellation process with projection areas and subcortical targets

Figure 2 shows a flowchart of the method. Following segmentation of the ROIs, the subcortical targets were exported and binarized as "3D objects". Then, the subcortical targets, processed as 3D objects, were imported back and coregistered into the working session as independent MRI series. In the "view section" of the software, we used the suggested range of DTI values and generated tracts from the projection areas under a neuroanatomical appraisal. The generated tracts were subjected to multiplanar reconstruction (MPR) and then used in the segmentation section in which we selected the subcortical target that we wanted to parcellate, which had been previously imported as a MRI series. With the subcortical target in the background and with the "selection tool", we selected the voxels located in the intersection between the outlined tract and the subcortical target, and thus, we were able to generate this region as an independent 3D object (Figs. 3 and 4).

Frameless stereotactic surgery

One day before surgery, seven fiducial markers of the frameless stereotactic system (Nexframe, Medtronic) were fixed onto the patient's skull under local anesthesia. Then, a CT scan was performed and the image data were transferred to the operating room and fused with the preoperative MRI studies using the Framelink® software 5.1 (Medtronic, Iberica, Spain). The initial target was determined using the AC-PC reference system according to the Schaltenbrand and Wahren atlas [54]. The structures targeted were STN for PD and VIM for essential tremor (ET) (coordinates are shown in Table 2). The optimal trajectory was chosen to avoid the vessels, sulci, and ventricles. Duraseal® (Integra LifeSciences Services, France) was used to plug the burr holes to avoid CSF egress. The final electrode position was determined by microelectrode recording (MER), micro and macrostimulation. The sites showing the most typical STN spike activity in the MER were tested with micro and macrostimulation for neurological

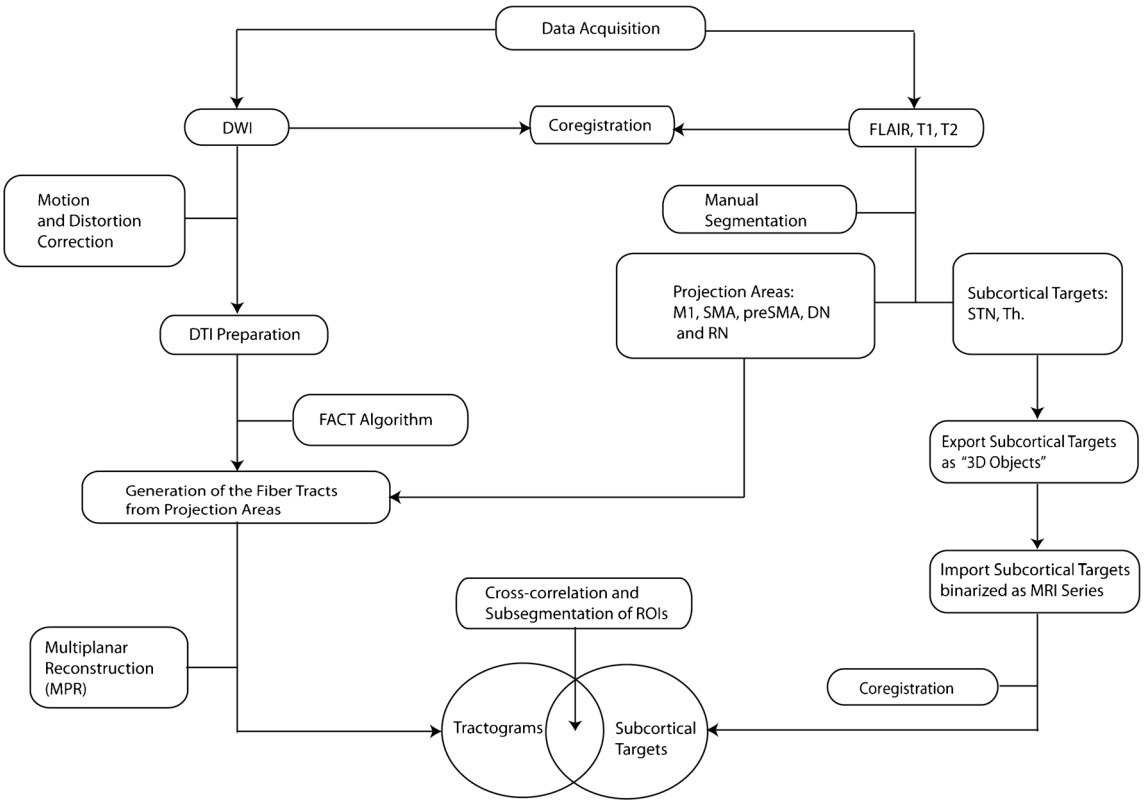

Fig. 2 Flowchart of the method used for localization of deep brain stimulation targets. *DN* dentate nucleus, *DTI* diffusion tensor image, *DWI* diffusion-weighted image, *FACT* fiber assignment by continuous tracking, *M1* primary motor cortex, *pre-SMA* pre-supplementary motor area, *RN* red nucleus, *SMA* supplementary motor area, *STN* subthalamic nucleus, *Th* thalamus

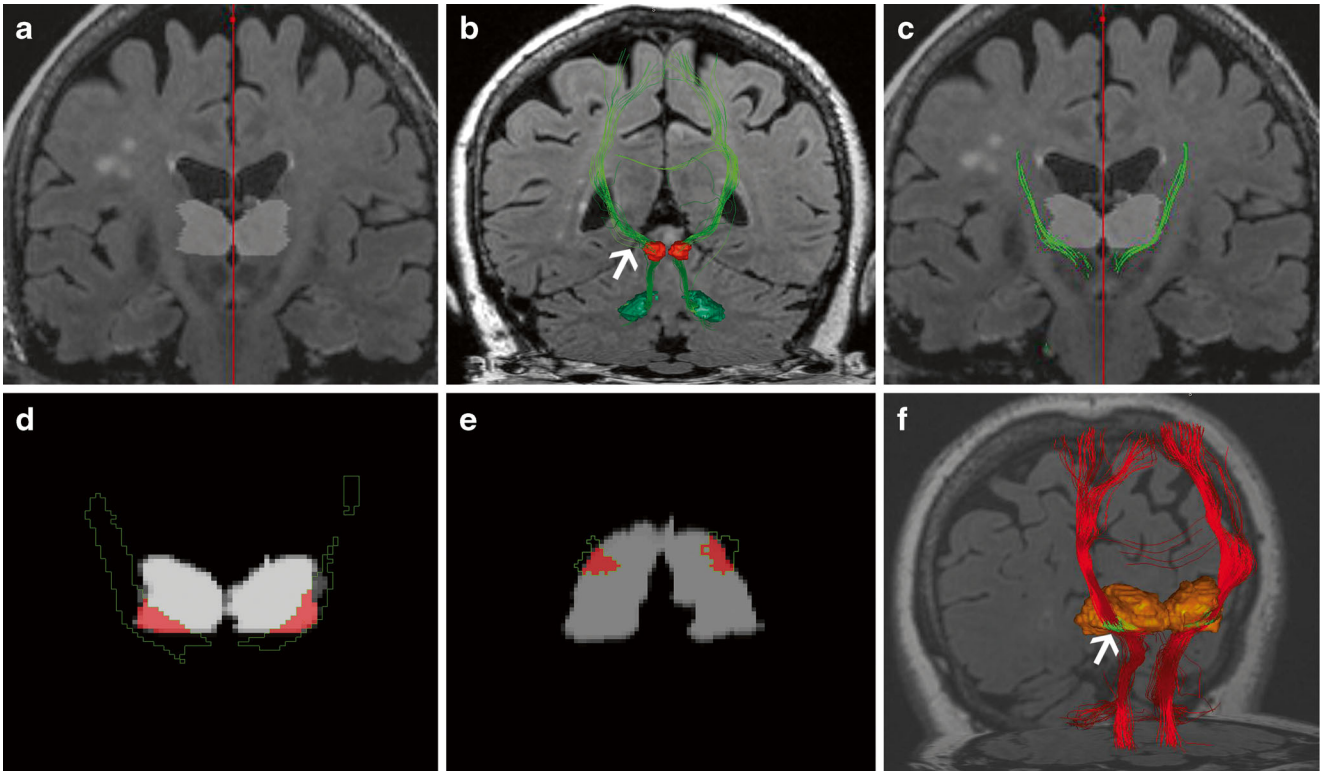

Fig. 3 Identification of the optimized target of the thalamus (Th) for patients with essential tremor. **a** The thalamus (*white region*) was fused with the structural magnetic resonance image (MRI). **b** The tracts were generated through projections from the dentate nucleus (DN) (*green*) and red nucleus (RN) (*red*); the dentatorubrothalamic tract is also identified (*arrow*). **c** The "3D lines" (*fibers in green*) obtained were superimposed with the fusion. **d** Coronal view, multiplanar reconstruction of the tract (*green*) in the segmentation section of the software. In this way, we were able to choose the voxels in the intersection between the thalamus and the reconstructed tract (*red voxels*). **e** Axial view of **d. f** Patient 8. The 3D renderization of the thalamus and the region obtained by our method is shown in green (*arrow*). The projections from this area replicate the known connections of the VIM nucleus (RN, DN, primary motor cortex, and supplementary motor area) [3, 11, 20, 33, 36]

symptom improvement and possible side effects. The trajectory was modified until MER and stimulation effects were satisfactory. The electrodes implanted were the reference 3389 from Medtronic. Finally, the patient underwent implantation of the pulse generator. Table 1 summarizes the stimulation parameters and clinical outcomes of the patients and the number of trajectories performed.

Comparison of the tractography-based OT and the atlas-based target with the clinically effective electrode contact

After surgery, a CT scan was performed and the images were fused with the MR preoperative planning. In the early postoperative period, a neurologist expert in

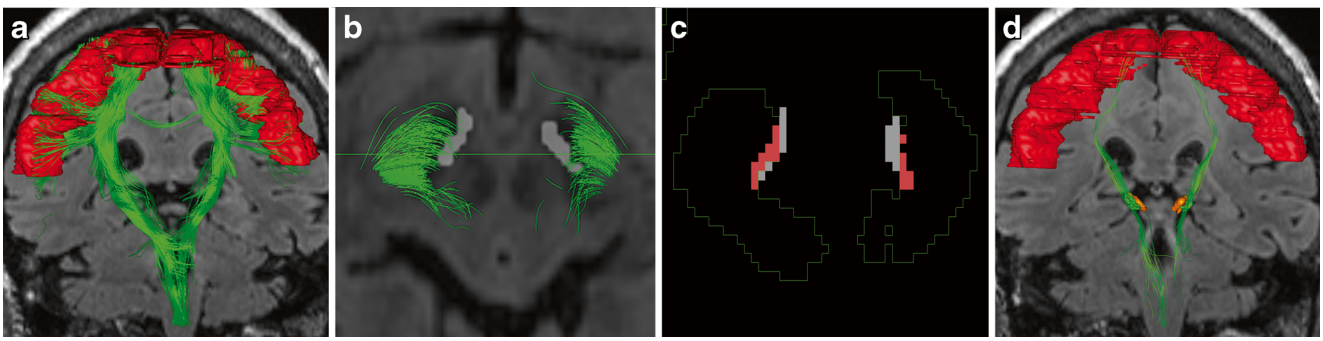

Fig. 4 Identification of the optimized target of the subthalamic nucleus (STN) for patients with Parkinson's disease. **a** Coronal view of the 3D tracking from the M1 and SMA-pre-SMA (*red*) showing the pyramidal tract (*green*). **b** The 3D lines (*fibers in green*) obtained were superimposed with the fusion of the segmented STN (*white*) and the structural MRI in axial view. **c** Axial view, multiplanar reconstruction of the tract (*green*) in the segmentation section of the software. In this way, we were able to choose the voxels in the intersection between the STN and the reconstructed tract (*red voxels*). **d** Patient 6. The 3D renderization of the STN and the region obtained by our method (*green*). The projections from this area replicate the corticosubthalamic connections, mainly with M1, and also with SMA and pre-SMA [16, 41]

Table 2 Relationship between atlas-based coordinates used for DBS with the coordinates of the optimized target (OT) obtained by our method and the clinically effective electrode contact. The coordinates are referenced from the AC-PC mid-commissural point

Patient/side	A coordinates (mm)			E coordinates (mm)			T coordinates (mm)		
	x	y	z	x	y	z	x	y	z
1/L	−12	−3	−4	−11	0	−2	−10	−2	−3
1/R	12	−3	−4	12	−1	0	11	−3	−1
2/L	−12	−3	−4	−8	−3	−4	−13	−4	−3
2/R	12	−3	−4	10	−2	−4	10	−2	−4
3/L	−12	−3	−4	−12	−3	−10	−12	−5	−6
3/R	12	−3	−4	12	−3	−6	12	−5	−5
4/L	−12	−3	−4	−10	−4	−4	−10	−3	−4
4/R	12	−3	−4	12	1	−2	12	−3	−2
5/L	−12	−3	−4	−9	−4	−6	−8	−3	−7
5/R	12	−3	−4	10	−3	−6	9	−1	−7
6/L	−12	−3	−4	−11	1	−3	−11	−2	−5
6/R	12	−3	−4	9	0	−3	10	0	−5
7/L	−13	−6	0	−13	−5	1	−11	5	0
7/R	13	−6	0	12	−3	1	13	−7	2
8/L	−13	−6	0	−15	−2	5	−14	−5	4
8/R	13	−6	0	16	−2	5	14	−5	5
9/L	−14	−6	0	−12	−4	6	−12	−7	2
9/R	14	−6	0	11	−4	6	11	−4	3

A atlas-based coordinates, *E* coordinates of the most clinically effective electrode contacts, *T* coordinates of the OT, *L* left, *R* right

movement disorders evaluated the patients and the most clinically effective and best-tolerated contact combination was selected. DBS was programmed with a constant current, which permits to avoid the effect of the changes in the impedance taking place after surgery [47]. After a clinical follow-up period (Table 1), the coordinates of the center of the cathodic pole of the clinically effective electrode contacts (CEEC) were determined measuring their distance to the AC-PC line and midline sagittal plane. The coordinates of the OT were determined as the geometrical center of the parcellation measuring their distance to the AC-PC line and midline sagittal plane. These groups of coordinates obtained (CEEC coordinates and OT coordinates) and the planned coordinates, based on Schaltenbrand-Wahren atlas, are summarized in Table 2. The Euclidean distance between the CEEC coordinates and those of the atlas-based target was measured as follows: atlas-based $\sqrt{(XA-XE)^2+(YA-YE)^2+(ZA-ZE)^2}$ where *A* is the atlas-based target coordinates and *E* is the CEEC coordinates (A-E distance). Similarly, the Euclidean distance between the CEEC coordinates and those of the tractography-based target (OT coordinates) was measured as follows: $\sqrt{(XT-XE)^2+(YT-YE)^2+(ZT-ZE)^2}$ where *T* is the tractography-based target coordinates and *E* is the CEEC coordinates (T-E distance). Table 3 shows both the T-E and A-E distances and their difference for each case by side.

Table 3 Euclidean distance transformation of the coordinates

Patient/side	T-E distance (mm)	A-E distance (mm)	A-E T-E dif. (mm)
1/L	2.45	3.74	1.29
1/R	2.45	4.47	2.02
2/L	5.20	4.00	−1.20
2/R	0.00	2.24	2.24
3/L	4.47	6.00	1.53
3/R	2.24	2.00	−0.24
4/L	1.00	2.24	1.24
4/R	4.00	4.47	0.47
5/L	1.73	3.74	2.01
5/R	2.45	2.83	0.38
6/L	3.61	4.24	0.64
6/R	1.41	4.36	2.94
7/L	2.24	1.41	−0.82
7/R	4.24	3.32	−0.93
8/L	3.32	6.71	3.39
8/R	3.61	7.07	3.47
9/L	5.00	6.63	1.63
9/R	3.00	7.00	4.00

T-E optimized target and clinically effective electrode contact distance, *A-E* atlas-based target and clinically effective electrode contact distance, *dif* difference between distances, *L* left, *R* right

Statistical analysis

Statistical data analysis was done using STATA software package version 12.0 (TS, USA). Wilcoxon signed-rank test was used to compare each distance and the median of the distances, with $p<0.05$ considered as statistically significant.

Results

The patients were six males and three females, with a median age of 60 years. The surgical indications were medically resistant PD in six cases and medically resistant essential tremor (ET) in three cases. All patients showed significant clinical improvement with the stimulation, and there were no complications in the DBS procedures (Table 1).

The motor division of the STN was parcellated using the projections from M1, SMA, and pre-SMA. The regions obtained were mainly encountered in the dorsolateral part of the STN (Figs. 4 and 5). The projections from the DN, using the RN as "mid region" for the tracking, were used to reconstruct the dentate-rubro-thalamic (DRT) tract. This tract was found to be passing the Th through its infero-lateral border and was used for parcellation of the VIM nucleus (Figs. 3 and 5).

In eight patients and 14 electrodes (patient 2 right side, patient 3 left side), the T-E (tractography-based target-CEEC) distance was shorter than the A-E (atlas-based target-CEEC) distance (Figs. 6 and 7). In the left side of patient 2 and the right side of patient 3, the A-E distance was shorter than the T-E distance; and in patient 7, the A-E distance was shorter than the T-E distance bilaterally. The median T-E distance (IQ range) was 2.72 mm (2.23–4.00 mm), and the median A-E distance (IQ range) was 4.12 mm (2.82–6.00 mm) (Fig. 8). Wilcoxon's test showed that the T-E distance was significantly shorter ($p=0.003$) than the A-E distance in the majority of the patients with a positive difference, suggesting that the areas obtained by our method are more closely related with the most clinically accurate location than the first location planned at the beginning of the surgery (Fig. 8) (The raw data are summarized in Tables 3 and 4).

Discussion

Our present study describes a method for parcellation of DBS targets using DTI-DT implemented by a widely used navigation system (StealthStation® and StealthViz® software packages). With this method, we were able to identify an OT within the DBS target nuclei, such as the motor part of the STN and the VIM nucleus of the Th. An advantage of this method is that it could be entirely performed by a functional neurosurgeon using a commercially available surgical navigation system and clinically available MR sequences. There are other surgical planning workstations in the market such as Surgiplan® by Leksell stereotactic system. In this software, it is not possible to generate tracts from DTI information. However, this software offers image fusion tools, which enable to import the OT (obtained by tractography) as a digital imaging and communications in medicine (DICOM) file. This allows to coregister the OT with the structural MRI of the patient in order to be used during DBS surgery [44, 61].

The current techniques for targeting in DBS are based on atlases with a reported accuracy similar to the direct targeting in 3 T machines [58]. In the case of the STN, the contour of this structure in high-field MR machines, or the boundary of the red nucleus, is used by several authors to improve this

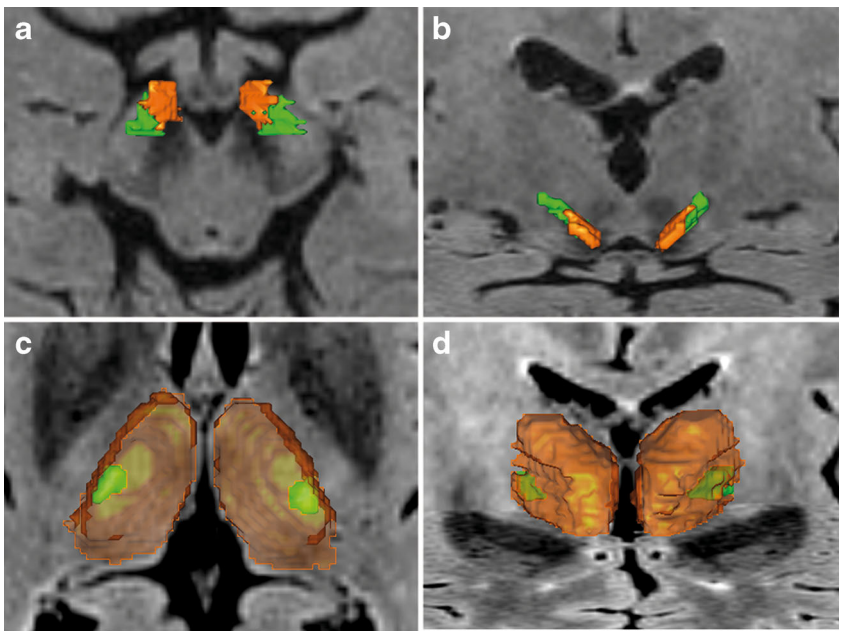

Fig. 5 Optimized target of the STN and Th of patients with Parkinson's disease and essential tremor. **a** Patient 4. Axial view, the subthalamic nucleus (STN) is shown (*orange* + *green*), the *green area* is the segment obtained by projections from M1, SMA, and pre-SMA. **b** Coronal view of **a**. It is important to note that the projections are mainly located at the dorsolateral region of the STN coincident with the motor part of the STN. **c** Patient 2. Axial view, the thalamus (Th) is shown (*orange* + *green*), and the projections from the dentate nucleus and the red nucleus are depicted in *green*. **d** Coronal view of **c**

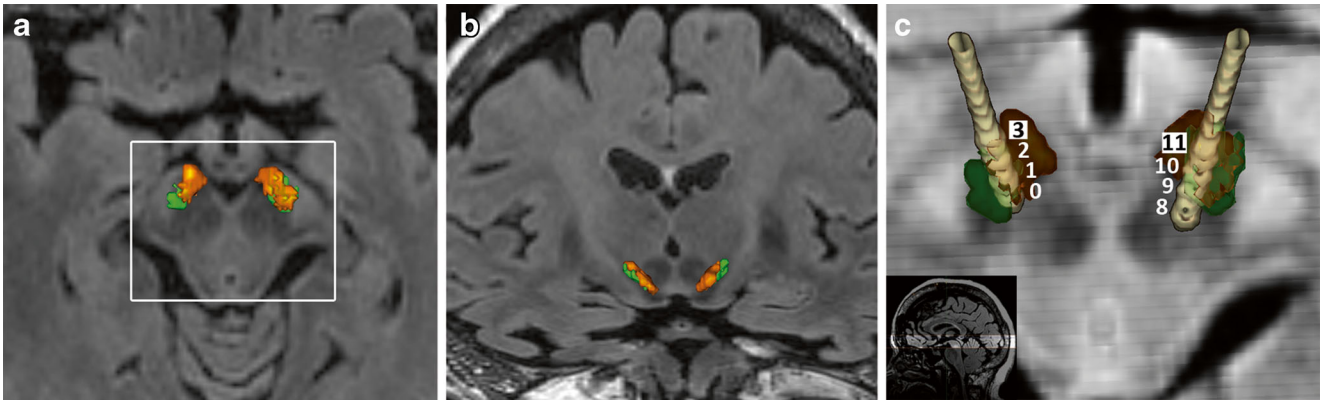

Fig. 6 Patient 6 (Parkinson's disease and target in the subthalamic nucleus (STN)). **a** Structural MRI showing the optimized target (OT) of the STN (*green*) obtained by our method. **b** Coronal view of **a. c** A zoom of the subthalamic area of the patient in **a** (*white inset*) with the electrodes superimposed; the *green areas* are the OT of the STN obtained by our method. We found that the most clinically effective electrode contacts are in close relation with the OT

accuracy [1, 5]. Direct visualization of the STN is a possibility to select the target [52]. Division of the directly visualized STN into four quadrants could be used to identify the dorsolateral part of the STN, where stimulation obtains the best clinical outcomes [67]. However, Coenen and coworkers [21], using an anatomo-radiologic analysis in a cadaver brain, showed that the sensoriomotor part of the nucleus is located at both the dorsolateral and *anterior* STN. Thus, a geometrical parcellation of the STN would not be sufficient to define the optimal target [57]. We would propose our method as an improvement of the direct visualization method since it uses the MR-defined STN to determine its intersection with the projection of the hyperdirect pathway defined by DTI-DT.

To interpret our results, we considered the best clinically effective electrode contact (CEEC) as the reference and compared its location with the atlas-based target and with the

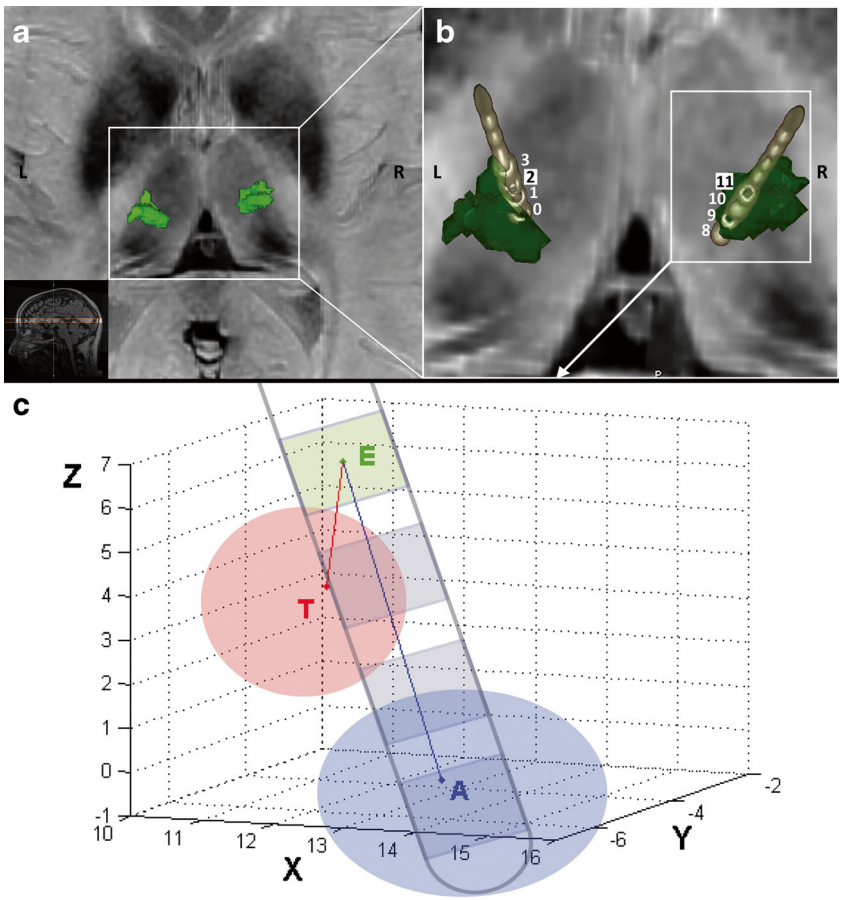

Fig. 7 Patient 9 (essential tremor and ventral intermediate nucleus (VIM)). **a** Structural MRI showing the optimized target (OT) of the thalamus (*green*) obtained by our method. **b** A zoom of the thalamic area of the patient in **a** (*white inset*) with the electrodes superimposed. This patient was operated for medically refractory essential tremor with bilateral VIM nucleus DBS. Postsurgical CT scan was fused with MRI. The clinically effective electrode contacts (CEEC) (L with contact 2 and R with contact 11) are coincident with the OT obtained by our method. **c** 3D surface plot with cartesian coordinates (x, y, z) to illustrate the study design with the electrode of the right side of the patient in **b**: Clinically effective electrode contact (*E*) is shown in *green*, tractography-based target (*T*) is shown in *red*, and atlas-based target (*A*) in *blue*. The distance between T and E is the *red line*, and the distance between A and E is the *blue line*

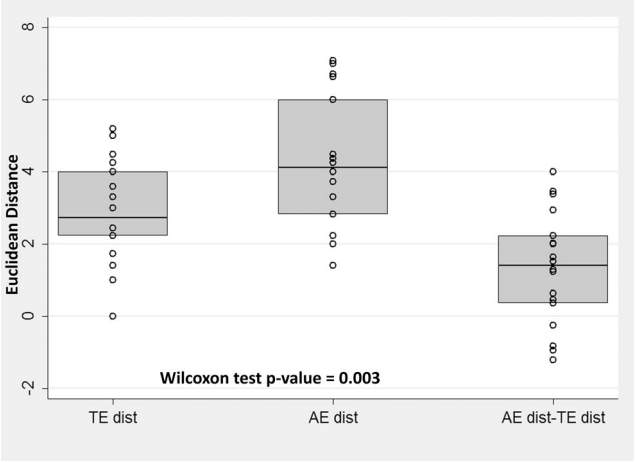

Fig. 8 Statistical comparisons of the Euclidean distance T-E vs A-E. Dot plots and box plots overlaid. The *boxplots* show the median distance corresponding to T-E and A-E and the difference of the distances between A-E and T-E. The *dots* show the individual values of all observations. *TE dist* optimized target and clinically effective electrode contact distance, *AE dist* atlas-based target and clinically effective electrode contact distance. *AE dist-TE dist* difference of the distance between AE and TE

target defined by our method (OT). Our results show that, in most patients (eight patients and 14 electrodes), the OT obtained by our method is more closely related with the CEEC than the atlas-based target (Fig. 8). Also, we found that there is more variance in the distribution of the A-E distances; this result is explained by the need of performing multiple trajectories during DBS surgery to obtain the clinically and neurophysiologically reliable site for stimulation. Finally, we found that the difference between the A-E distance and the T-E distance is mainly positive, suggesting that the target obtained by our method is more accurate as long as we consider the CEEC as the reference measure for effective targeting.

Many methods have been described to parcellate subcortical structures in humans using different algorithms [4, 11, 18, 25, 26, 41]. Behrens et al. described a fully probabilistic algorithm method for human thalamus parcellation, and others have used this method to parcellate other subcortical structures and even for targeting [11, 41, 43, 51]. Here, we used deterministic tractography under the "knowledge-based approach" described by Mori et al. [45], applying neuroanatomical knowledge to assess the generated tracts [29]. DTI is a newly available resource to optimize DBS targeting preoperatively in an individualized fashion [19, 20, 22]. Colored FA maps have been used to identify certain DBS targets by recognizing the major tracts connected to these targets, yielding the maximum anatomical information from this available MRI sequence that is scarcely utilized in clinical practice [55, 56]. Connectivity-based approaches for DBS targeting using probabilistic tractography have recently been assessed and validated in clinical practice and promise to be superior to indirect methods [27, 51, 60]. The efficient use of connectivity-based approaches will depend on the armamentarium for high-order imaging acquisition and software-related resources to achieve individualized targeting. The recent development of these techniques has changed the paradigm of DBS surgery, providing new insight into the rationale of DBS targeting and the understanding of the stimulation mechanism on subcortical networks.

To optimize targeting, functional subdivisions in the STN have been explored [9, 16, 41, 66]; for example, impulse control disorders are related to stimulation of a more ventromedial location of the electrode (the limbic STN) [34, 53]. With our novel method, we were able to identify the motor STN, as well as the limbic STN, which has been proposed as a target in OCD (data not shown) [13, 14, 17, 35, 39]. There is some debate over the optimal targeting in using DBS for tremor [49, 65]. The subdivisions of the thalamus cannot be directly visualized on 1.5 and 3 T MR machines. The location of the interface between the VIM nucleus and the ventralis caudalis (VC) nucleus—which is the primary somatosensory integration center—is critical because stimulation close to the interface may cause intolerable paresthesias [49]. We were able to identify the region coincident with the VIM nucleus using the projection from DN and RN, which could enable the

Table 4 Descriptive statistics of the distances

Side	Statistics	T-E distance (mm)	A-E distance (mm)	A-E T-E dif. (mm)
Left	p50	2.45	3.74	1.29
	p25	1.98	2.12	−0.09
	p75	3.46	5.47	1.82
Right	p50	3.61	4.47	2.02
	p25	1.93	3.07	0.07
	p75	4.35	6.31	3.20
Total	p50	2.72	4.12	1.41
	p25	2.23	2.82	0.37
	p75	4.00	6.00	2.23

T-E optimized target and clinically effective electrode contact distance, *A-E* atlas-based target and clinically effective electrode contact distance, *dif* difference between distances

avoidance of stimulation paresthesias via direction of the electrode to a site far from the posterior border of the parcellation. We could also identify the location of the DRT tract, thus enabling stimulation optimization by placement of the electrode in a close relation with this tract [19, 20, 22, 36].

The main limitation of this work was the small number of patients involved, which made it difficult to correlate clinical results. However, the purpose of this paper is not to establish DTI as a standard procedure to determine targets but to describe the method and show its feasibility. Another limitation of this technique can be the interindividual variability and the reproducibility of the method, since the determination of the structures is subjective. Also, the manual segmentation process is time consuming and requires expertise in the use of planning station software; however, the software includes many tools and functions that could reduce the time required to perform this method. Some software allows automated parcellation that requires further adjustment of the cortical masks generated to deal with interindividual variability of the cortical gyri [24, 25]. A main advantage of this method is its simplicity, which lowers the need of human and computational resources.

Also, DTI technology must be used with caution. A single-tensor model (even with multiple directions) cannot describe the reality of huge voxels (2.6 mm) that have multiple fiber populations. So, the DTI values of the voxels must not be taken exactly as the real white matter populations that are intended to represent. Also, this low resolution of DTI could lead to interpret fibers belonging to nearby structures (e.g., the internal capsule) as fibers specific from the target structure (for example, the STN). However, our tractography-based target is defined by the intersection of the DTI fibers (from the projection areas) and the anatomical STN or Th (subcortical targets). Therefore, any voxel belonging to outside the STN or the Th (i.e., the internal capsule) would be avoided during the segmentation process. Distortion could shadow the anatomical accuracy; however, we used Functool® software to deal with the geometric distortion [8, 12, 45]. Additionally, the diffusively overlapping nature of the basal ganglia connections can limit the tracing of segregated loops throughout the cortico-subcortical circuits [26, 43]. Furthermore, it is not possible to determine the polarity of the fibers using DTI [11, 26]. Another limitation appears when an image voxel contains fiber populations with more than one dominant orientation [28]. However, neuroanatomical knowledge can enable the rejection of a misled group of generated fibers [29, 45]. Accumulated uncertainties in fiber orientation have clear a potential for leading to erroneous pathway reconstructions [12]. Probabilistic methods might adequately deal with some of these limitations [8, 10]. Moreover, the precision of the technique is still limited by the MR voxel size (around 1 mm) and the precision of the stereotactic instrument (about 0.5 mm). Brain shift due to the outflow of CSF could also distort the target location especially in the second treatment side. However, this would affect both the atlas-based target and the optimized target. Measures to minimize CSF egress must be taken such as plugging the burr holes with glue. These considerations also suggest that neurophysiological confirmation cannot be replaced by the procedure presented here.

The presently described method is not intended as a substitute for neurophysiological confirmation of the target but as a means of starting the targeting with a more individualized *initial estimate*. It could also be particularly helpful in patients who do not tolerate an awake surgery. Further investigation in a larger population is needed to determine if this method is more accurate than the standard atlas or plain MR image-based targeting methods.

Conclusions

Our results show that identification of the OT within the DBS target nuclei is feasible with our novel method. Based on neural circuits, we obtained plausible results that were consistent with clinical data in a group of patients, although prospective and controlled studies are necessary to demonstrate its beneficial role. The newly described method is straightforward and is entirely performed using available navigation software, with the possibility to use these regions during surgery as additional landmarks or to post-surgically explore the results of stimulation.

Acknowledgments This work was supported by Instituto de Salud Carlos III, grant number PI10/1932. The authors thank Dr. Juan Alvarez-Linera for the image acquisition, Juan Sobrado and Julio Gonzalez for the technical support in the software, and Mrs. Ingrid Carranza for the support and assistance in the figures, tables, and illustrations.

Disclosures The authors have no personal financial or institutional interest in any of the materials or devices described in this article.

References

1. Abosch A, Timmermann L, Bartley S, Rietkerk HG, Whiting D, Connolly PJ, Lanctin D, Hariz MI (2013) An international survey of deep brain stimulation procedural steps. Stereotact Funct Neurosurg 91(1):1–11
2. Abosch A, Yacoub E, Ugurbil K, Harel N (2010) An assessment of current brain targets for deep brain stimulation surgery with susceptibility-weighted imaging at 7 tesla. Neurosurgery 67(6): 1745–1756, **discussion 1756**
3. Akakin A, Peris-Celda M, Kilic T, Seker A, Gutierrez-Martin A, Rhoton A (2014) The dentate nucleus and its projection system in

the human cerebellum: the dentate nucleus microsurgical anatomical study. Neurosurgery 74(4):401–425
4. Anderson JS, Dhatt HS, Ferguson MA, Lopez-Larson M, Schrock LE, House PA, Yurgelun-Todd D (2011) Functional connectivity targeting for deep brain stimulation in essential tremor. AJNR Am J Neuroradiol 32(10):1963–1968
5. Andrade-Souza YM, Schwalb JM, Hamani C, Eltahawy H, Hoque T, Saint-Cyr J, Lozano AM (2005) Comparison of three methods of targeting the subthalamic nucleus for chronic stimulation in Parkinson's disease. Neurosurgery 56(2 Suppl):360–368, **discussion 360–8**
6. Aravamuthan BR, Muthusamy KA, Stein JF, Aziz TZ, Johansen-Berg H (2007) Topography of cortical and subcortical connections of the human pedunculopontine and subthalamic nuclei. Neuroimage 37(3):694–705
7. Barbe MT, Liebhart L, Runge M, Deyng J, Florin E, Wojtecki L, Schnitzler A, Allert N, Sturm V, Fink GR, Maarouf M, Timmermann L (2011) Deep brain stimulation of the ventral intermediate nucleus in patients with essential tremor: stimulation below intercommissural line is more efficient but equally effective as stimulation above. Exp Neurol 230(1):131–137
8. Basser PJ, Jones DK (2002) Diffusion-tensor MRI: theory, experimental design and data analysis—a technical review. NMR Biomed 15(7–8):456–467
9. Baudrexel S, Witte T, Seifried C, von Wegner F, Beissner F, Klein JC, Steinmetz H, Deichmann R, Roeper J, Hilker R (2011) Resting state fMRI reveals increased subthalamic nucleus-motor cortex connectivity in Parkinson's disease. Neuroimage 55(4):1728–1738
10. Behrens TEJ, Berg HJ, Jbabdi S, Rushworth MFS, Woolrich MW (2007) Probabilistic diffusion tractography with multiple fibre orientations: what can we gain? Neuroimage 34(1):144–155
11. Behrens TEJ, Johansen-Berg H, Woolrich MW, Smith SM, Wheeler-Kingshott CA, Boulby PA, Barker GJ, Sillery EL, Sheehan K, Ciccarelli O, Thompson AJ, Brady JM, Matthews PM (2003) Non-invasive mapping of connections between human thalamus and cortex using diffusion imaging. Nat Neurosci 6(7):750–757
12. Behrens TEJ, Woolrich MW, Jenkinson M, Johansen-Berg H, Nunes RG, Clare S, Matthews PM, Brady JM, Smith SM (2003) Characterization and propagation of uncertainty in diffusion-weighted MR imaging. Magn Reson Med 50(5):1077–1088
13. Benabid AL, Torres N (2012) New targets for DBS. Parkinsonism Relat Disord 18(Suppl 1):S21–S23
14. Benarroch EE (2008) Subthalamic nucleus and its connections: anatomic substrate for the network effects of deep brain stimulation. Neurology 70(21):1991–1995
15. Blomstedt P, Sandvik U, Tisch S (2010) Deep brain stimulation in the posterior subthalamic area in the treatment of essential tremor. Mov Disord 25(10):1350–1356
16. Brunenberg EJL, Moeskops P, Backes WH, Pollo C, Cammoun L, Vilanova A, Janssen MLF, Visser-Vandewalle VERM, ter Haar Romeny BM, Thiran J-P, Platel B (2012) Structural and resting state functional connectivity of the subthalamic nucleus: identification of motor STN parts and the hyperdirect pathway. PLoS One 7(6), e39061
17. Chabardès S, Polosan M, Krack P, Bastin J, Krainik A, David O, Bougerol T, Benabid AL (2012) Deep brain stimulation for obsessive-compulsive disorder: subthalamic nucleus target. World Neurosurg 80:1–8
18. Chowdhury R, Lambert C, Dolan RJ, Düzel E (2013) Parcellation of the human substantia nigra based on anatomical connectivity to the striatum. Neuroimage 81:191–198
19. Coenen VA, Allert N, Mädler B (2011) A role of diffusion tensor imaging fiber tracking in deep brain stimulation surgery: DBS of the dentato-rubro-thalamic tract (drt) for the treatment of therapy-refractory tremor. Acta Neurochir (Wien) 153(8): 1579–1585, **discussion 1585**
20. Coenen VA, Mädler B, Schiffbauer H, Urbach H, Allert N (2011) Individual fiber anatomy of the subthalamic region revealed with diffusion tensor imaging: a concept to identify the deep brain stimulation target for tremor suppression. Neurosurgery 68(4):1069–1075, **discussion 1075–6**
21. Coenen VA, Prescher A, Schmidt T, Picozzi P, Gielen FLH (2008) What is dorso-lateral in the subthalamic nucleus (STN)?—a topographic and anatomical consideration on the ambiguous description of today's primary target for deep brain stimulation (DBS) surgery. Acta Neurochir (Wien) 150(11):1163–1165, **discussion 1165**
22. Coenen VA, Schlaepfer TE, Allert N, Mädler B (2012) Diffusion tensor imaging and neuromodulation: DTI as key technology for deep brain stimulation. Int Rev Neurobiol 107:207–234
23. DeLong MR, Wichmann T (2007) Circuits and circuit disorders of the basal ganglia. Arch Neurol 64(1):20–24
24. Desikan RS, Ségonne F, Fischl B, Quinn BT, Dickerson BC, Blacker D, Buckner RL, Dale AM, Maguire RP, Hyman BT, Albert MS, Killiany RJ (2006) An automated labeling system for subdividing the human cerebral cortex on MRI scans into gyral based regions of interest. Neuroimage 31(3):968–980
25. Destrieux C, Fischl B, Dale A, Halgren E (2010) Automatic parcellation of human cortical gyri and sulci using standard anatomical nomenclature. Neuroimage 53(1):1–15
26. Draganski B, Kherif F, Klöppel S, Cook PA, Alexander DC, Parker GJM, Deichmann R, Ashburner J, Frackowiak RSJ (2008) Evidence for segregated and integrative connectivity patterns in the human basal ganglia. J Neurosci 28(28):7143–7152
27. Elias WJ, Zheng ZA, Domer P, Quigg M, Pouratian N (2012) Validation of connectivity-based thalamic segmentation with direct electrophysiologic recordings from human sensory thalamus. Neuroimage 59(3):2025–2034
28. Farquharson S, Tournier J-D, Calamante F, Fabinyi G, Schneider-Kolsky M, Jackson GD, Connelly A (2013) White matter fiber tractography: why we need to move beyond DTI. J Neurosurg 118(6):1367–1377
29. Fernandez-Miranda JC, Pathak S, Engh J, Jarbo K, Verstynen T, Yeh F-C, Wang Y, Mintz A, Boada F, Schneider W, Friedlander R (2012) High-definition fiber tractography of the human brain: neuroanatomical validation and neurosurgical applications. Neurosurgery 71(2): 430–453
30. Fuster JM (2008) The prefrontal cortex, Fourth ed. 7–44
31. Guridi J, Rodríguez-Oroz MC, Ramos E, Linazasoro G, Obeso JA (2002) Discrepancy between imaging and neurophysiology in deep brain stimulation of medial pallidum and subthalamic nucleus in Parkinson's disease. Neurologia 17(4):183–192
32. Gutman DA, Holtzheimer PE, Behrens TEJ, Johansen-Berg H, Mayberg HS (2009) A tractography analysis of two deep brain stimulation white matter targets for depression. Biol Psychiatry 65(4):276–282
33. Hamani C, Dostrovsky JO, Lozano AM (2006) The motor thalamus in neurosurgery. Neurosurgery 58(1):146–158
34. Hamani C, Saint-Cyr JA, Fraser J, Kaplitt M, Lozano AM (2004) The subthalamic nucleus in the context of movement disorders. Brain 127(Pt 1):4–20
35. Haynes WI, Mallet L (2010) High-frequency stimulation of deep brain structures in obsessive-compulsive disorder: the search for a valid circuit. Eur J Neurosci 32(7):1118–1127
36. Hyam JA, Owen SLF, Kringelbach ML, Jenkinson N, Stein JF, Green AL, Aziz TZ (2012) Contrasting connectivity of the ventralis intermedius and ventralis oralis posterior nuclei of the motor thalamus demonstrated by probabilistic tractography. Neurosurgery 70(1):162–169, **discussion 169**
37. Jiang H, van Zijl PCM, Kim J, Pearlson GD, Mori S (2006) DtiStudio: resource program for diffusion tensor computation and

fiber bundle tracking. Comput Methods Programs Biomed 81(2): 106–116
38. Klein JC, Rushworth MFS, Behrens TEJ, Mackay CE, de Crespigny AJ, D'Arceuil H, Johansen-Berg H (2010) Topography of connections between human prefrontal cortex and mediodorsal thalamus studied with diffusion tractography. Neuroimage 51(2):555–564
39. Kopell BH, Greenberg BD (2008) Anatomy and physiology of the basal ganglia: implications for DBS in psychiatry. Neurosci Biobehav Rev 32(3):408–422
40. Kopell BH, Rezai AR, Chang JW, Vitek JL (2006) Anatomy and physiology of the basal ganglia: implications for deep brain stimulation for Parkinson's disease. Mov Disord 21(Suppl 1):S238–S246
41. Lambert C, Zrinzo L, Nagy Z, Lutti A, Hariz M, Foltynie T, Draganski B, Ashburner J, Frackowiak R (2012) Confirmation of functional zones within the human subthalamic nucleus: patterns of connectivity and sub-parcellation using diffusion weighted imaging. Neuroimage 60(1):83–94
42. Lehéricy S, Ducros M, Krainik A, Francois C, Van de Moortele P-F, Ugurbil K, Kim D-S (2004) 3-D diffusion tensor axonal tracking shows distinct SMA and pre-SMA projections to the human striatum. Cereb Cortex 14(12):1302–1309
43. Lenglet C, Abosch A, Yacoub E, De Martino F, Sapiro G, Harel N (2012) Comprehensive in vivo mapping of the human basal ganglia and thalamic connectome in individuals using 7 T MRI. PLoS One 7(1), e29153
44. Maruyama K, Koga T, Kamada K, Ota T, Itoh D, Ino K, Igaki H, Aoki S, Masutani Y, Shin M, Saito N (2009) Arcuate fasciculus tractography integrated into Gamma Knife surgery. J Neurosurg 111(3):520–526
45. Mori S, van Zijl PCM (2002) Fiber tracking: principles and strategies—a technical review. NMR Biomed 15(7–8):468–480
46. Nieuwenhuys R, Voogd J, Van Huijzen C (2008) The human central nervous system. 253–286, 427–653
47. Okun MS, Gallo BV, Mandybur G et al (2012) Subthalamic deep brain stimulation with a constant-current device in Parkinson's disease: an open-label randomised controlled trial. Lancet Neurol 11(2):140–149
48. Ongür D, Ferry AT, Price JL (2003) Architectonic subdivision of the human orbital and medial prefrontal cortex. J Comp Neurol 460(3):425–449
49. Papavassiliou E, Rau G, Heath S, Abosch A, Barbaro NM, Larson PS, Lamborn K, Starr PA (2004) Thalamic deep brain stimulation for essential tremor: relation of lead location to outcome. Neurosurgery 54(5):1120–1130
50. Parent A, Lévesque M, Parent M (2001) A re-evaluation of the current model of the basal ganglia. Parkinsonism Relat Disord 7(3):193–198
51. Pouratian N, Zheng Z, Bari AA, Behnke E, Elias WJ, Desalles AA (2011) Multi-institutional evaluation of deep brain stimulation targeting using probabilistic connectivity-based thalamic segmentation. J Neurosurg 115(5):995–1004
52. Richter EO, Hoque T, Halliday W, Lozano AM, Saint-Cyr JA (2004) Determining the position and size of the subthalamic nucleus based on magnetic resonance imaging results in patients with advanced Parkinson disease. J Neurosurg 100(3):541–546
53. Rodriguez-Oroz MC, López-Azcárate J, Garcia-Garcia D, Alegre M, Toledo J, Valencia M, Guridi J, Artieda J, Obeso JA (2011) Involvement of the subthalamic nucleus in impulse control disorders associated with Parkinson's disease. Brain 134(Pt 1):36–49
54. Schaltenbrand G, Wahren W (1977) Atlas for stereotaxy of the human brain. Second ed. Thieme, Stuttgart
55. Sedrak M, Gorgulho A, Bari A, Behnke E, Frew A, Gevorkyan I, Pouratian N, DeSalles A (2010) Diffusion tensor imaging (DTI) and colored fractional anisotropy (FA) mapping of the subthalamic nucleus (STN) and the globus pallidus interna (GPi). Acta Neurochir (Wien) 152(12):2079–2084
56. Sedrak M, Gorgulho A, Frew A, Behnke E, DeSalles A, Pouratian N (2011) Diffusion tensor imaging and colored fractional anisotropy mapping of the ventralis intermedius nucleus of the thalamus. Neurosurgery 69(5):1124–1129, **discussion 1129–30**
57. Shenai MB, Romeo A, Walker HC, Guthrie S, Watts RL, Guthrie BL (2015) Spatial topographies of unilateral subthalamic nucleus deep brain stimulation efficacy for ipsilateral, contralateral, midline, and total Parkinson disease motor symptoms. Neurosurgery 00(00):8–14
58. Stancanello J, Muacevic A, Sebastiano F, Modugno N, Cerveri P, Ferrigno G, Uggeri F, Romanelli P (2008) 3 T MRI evaluation of the accuracy of atlas-based subthalamic nucleus identification. Med Phys 35(7):3069–3077
59. Sturm V, Lenartz D, Koulousakis A, Treuer H, Herholz K, Klein JC, Klosterkötter J (2003) The nucleus accumbens: a target for deep brain stimulation in obsessive–compulsive- and anxiety-disorders. J Chem Neuroanat 26(4):293–299
60. Sudhyadhom A, McGregor K, Okun MS, Foote KD, Trinastic J, Crosson B, Bova FJ (2013) Delineation of motor and somatosensory thalamic subregions utilizing probabilistic diffusion tractography and electrophysiology. J Magn Reson Imaging 37(3):600–609
61. Tamura M, Hayashi M, Konishi Y, Tamura N, Regis J, Mangin JF, Taira T, Okada Y, Muragaki Y, Iseki H (2013) Advanced image coregistration within the Leksell workstation for the planning of glioma surgery: initial experience. J Neurol Surg Rep 74(2):118–122
62. Toda H, Sawamoto N, Hanakawa T, Saiki H, Matsumoto S, Okumura R, Ishikawa M, Fukuyama H, Hashimoto N (2009) A novel composite targeting method using high-field magnetic resonance imaging for subthalamic nucleus deep brain stimulation. J Neurosurg 111(4):737–745
63. Tomassini V, Jbabdi S, Klein JC, Behrens TEJ, Pozzilli C, Matthews PM, Rushworth MFS, Johansen-Berg H (2007) Diffusion-weighted imaging tractography-based parcellation of the human lateral premotor cortex identifies dorsal and ventral subregions with anatomical and functional specializations. J Neurosci 27(38):10259–10269
64. Utter AA, Basso MA (2008) The basal ganglia: an overview of circuits and function. Neurosci Biobehav Rev 32(3):333–342
65. Vaillancourt DE, Sturman MM, Verhagen Metman L, Bakay RA, Corcos DM (2003) Deep brain stimulation of the VIM thalamic nucleus modifies several features of essential tremor. Neurology 61(7):919–925
66. Vertinsky AT, Coenen VA, Lang DJ, Kolind S, Honey CR, Li D, Rauscher A (2009) Localization of the subthalamic nucleus: optimization with susceptibility-weighted phase MR imaging. AJNR Am J Neuroradiol 30(9):1717–1724
67. Wodarg F, Herzog J, Reese R, Falk D, Pinsker MO, Steigerwald F, Jansen O, Deuschl G, Mehdorn HM, Volkmann J (2012) Stimulation site within the MRI-defined STN predicts postoperative motor outcome. Mov Disord 27(7):874–879
68. Yamada K, Sakai K, Akazawa K, Yuen S, Nishimura T (2009) MR tractography: a review of its clinical applications. Magn Reson Med Sci 8(4):165–174
69. Yang Y, Raine A (2009) Prefrontal structural and functional brain imaging findings in antisocial, violent, and psychopathic individuals: a meta-analysis. Psychiatry Res 174(2): 81–88
70. Yelnik J, Bardinet E, Dormont D, Malandain G, Ourselin S, Tandé D, Karachi C, Ayache N, Cornu P, Agid Y (2007) A three-dimensional, histological and deformable atlas of the human basal ganglia. I. Atlas construction based on immunohistochemical and MRI data. Neuroimage 34(2):618–638
71. Zrinzo L (2010) The role of imaging in the surgical treatment of movement disorders. Neuroimaging Clin N Am 20(1):125–140

Comments

Tetsuya Goto, Matsumoto, Japan

The authors reported the useful target measuring method in deep brain stimulation surgery guided by MRI tractography. Their methodology looks reasonable and agreeable. They concluded that their advocating target was superior to using atlas-based target (x −12 mm, y −3 mm, z −4 mm from AC-PC line) because it was nearer to the most clinically effective electrode contact point than atlas-based target.

When the stereotactic surgery guided by microrecording is performed, the initial target should be determined by not only the final target point in the dorsolateral STN but also the insertion point, trajectory angle, ventricle size, and thickness of thalamus. The most clinically effective electrode contact point is not also the initial target because it is decided after checking the effectiveness of treatment and the complications of side effects. The authors moved the target two or three times, although they were guided by their method. The selection of the initial target might be discussed by the number of times of the trajectory.

If the direct visualization of the STN is possible by using their method, it may be superior to conventional technique. These techniques will shift the paradigm from the microrecording-guided to radiographic-guided stereotactic surgery. They will reduce the number of times of the trajectory, risk of hemorrhage, and operation time.

Peter Grunert, Homburg/Saar, Germany

An intrinsic problem in functional stereotaxy is the fact that in most of the cases, the target is not directly visible in the images neither in ventriculography nor in CT or in MRI. Therefore, indirect methods based on a human atlas have been developed to determine the target point in relation to defined anatomical landmarks such as the anterior and posterior commissure. Additionally, intraoperative microelectrode recording and electric stimulation were routinely intraoperatively applied during deep brain stimulation to optimize the target for the final placement of the electrode. The authors in this contribution proposed a new method for optimizing the target point by visualization of the afferent or efferent tracts to or from the target area. For the STN, they visualized the connections of this nucleus to the cortical motor and several premotor areas. For the VIM nucleus in the thalamus, they were able to demonstrate the efferent fibers from dentate and ruber nucleus to the area of the VIM. This was achieved in MRI images by the meanwhile established method of fiber tracking. Despite several technical limitations of this method, the authors could show that their optimized target calculation based on tractography was statically more close to the final target established by electrophysiological methods than the calculation based on a stereotactic atlas.

I think this is a very interesting and original contribution with great potential in the future. The tractography with the visualization of the well-known anatomical afferent and efferent connections seems to be a very logical and promising method to optimize the target even within the target area. In the future, with better image resolution, tractography may make the time-consuming electrophysiological testing superfluous. However, at this point of development, in particular for small target areas, the electrophysiological investigations are still indispensible.

Jürgen Voges, Magdeburg, Germany

This manuscript describes a procedure using deterministic tractography (DTI) to improve stereotactic targeting. The integration of DTI into stereotactic treatment planning protocols for DBS surgery seems logical because it is widely accepted that large fibers originating in or projecting onto the stimulated area play a prominent role in mediating the beneficial effects of neurostimulation. Referred to the here examined targets, crucial fiber tracts are the "hyperdirect pathway" in the case of the subthalamic nucleus or the "dentatorubrothalamic tract" (DRT) when the ventral intermediate thalamic nucleus is electrically stimulated. If direct targeting of fiber tracts instead of relais nuclei will improve the clinical outcome is not yet clearly defined. Schlaier and collaborators, for instance, addressing intraoperative tremor improvement as a function of the spatial relationship of active electrode contacts and the DRT, reported that the distance to this fiber tract had no impact on the outcome (1). The findings of Coenen et al., in contrast, displayed a trend for better tremor response when active electrode contacts projected onto the DRT in comparison to those contacts located at the anterior border of this tract, but this difference was statistically not significant (2).

General concerns, when using clinical tractography, refer to the anatomic accuracy of this method. Thomas and colleagues investigated in-depth the assumption that the combination of high-resolution diffusion-weighted imaging and sophisticated diffusion modeling approaches may provide anatomically correct connectivity maps of the brain. Comparing the "visualized" connections with those derived from tracer studies—the "gold standard"—this group demonstrated that suboptimal information accuracy results from inherent methodological limitations of tractography. According to their conclusions, comprehensive methodological modifications are required to overcome these limitations (3). Related to stereotactic treatment planning, tractography cannot replace electrophysiology and/or intraoperative clinical testing at that time, and keeping the aforementioned methodological problems in reference, it is recommended to use DTI skeptically.

References

1. Schlaier J, Anthofer J, Steib K, Fellner C, Rothenfusser E, Brawanski A, Lange M. Deep brain stimulation for essential tremor: targeting the dentato-rubro-thalamic tract? Neuromodulation 2014.

2. Coenen VA, Allert N, Paus S, Kronenburger M, Urbach H, Madler B. Modulation of the cerebello-thalamo-cortical network in thalamic deep brain stimulation for tremor: a diffusion tensor imaging study. Neurosurgery 2014;75:657–670.

3. Thomas C, Ye FQ, Irfanoglu MO, Modi P, Saleem KS, Leopold DA, Pierpaoli C. Anatomical accuracy of brain connections derived from diffusion MRI tractography is inherently limited. Proc Natl Acad Sci U S A 2014;111:16574–16579.